[1]Tilak Dhari Singh

[2] Shivesh Tripathi

[3] Kamal Prakash Pandey

[4]V. S. Tripathi

A planar Vivaldi Antenna based Microwave Imaging Sensor for Monitoring of Bone Fracture Healing

Journal of Electrical Systems

Abstract: - This study investigates a straight forward and useful technique for employing Microwave Imaging (MWI) in terms of frequency shift and variation in reflection coefficient to identify fractures in surface-level bones, such as the tibia. The technology is made to help first responders diagnose patients quickly in emergencies, particularly in locations lacking access to X-rays. Additionally, it is helpful in circumstances when X-rays are not advised, including for youngsters or pregnant women. The technology, which is based on antenna-based sensor, scans the bone in the 3.08–11.57 GHz frequency range using a single Vivaldi antenna. This system is useful and simple to use because it is compact with 28 mm in length, 29.1 mm in breadth, and 1.5 mm in height. Antenna is designed on Rogers RT/duroid 5880TM.

Keywords: Non-invasive, Vivaldi antenna, bone fracture, SAR, microwave imaging.

I. INTRODUCTION

Medical imaging procedures including X-rays, CT scans, and MRIs are typically used to identify and track bone fractures. Because they are readily available and reasonably priced, X-rays are the most often used of them. They might not, however, readily display minor or subtle fractures. Although they are costlier, CT and MRI scans provide more comprehensive images. While MRI is slower and more expensive, CT scans also employ dangerous radiation [1-2].

Fractures are extremely prevalent, particularly in older adults and children. For instance, tibia fractures, which occur in roughly 15% of cases, rank third among long bone fractures in children. Finding a less expensive, portable, and secure method of fracture detection is therefore crucial. Additionally, such a strategy would be useful in low-income communities, retirement homes, and ambulances. In situations where radiation exposure must be prevented, it may also be helpful for expectant mothers, new babies, and infants [3-4].

The concept behind this study is to employ microwave imaging as a non-invasive, safe method of detecting bone fractures. The suggested method detects alterations in the characteristics of the bone at the fracture site using microwave radiation [5]. The device can identify the fracture by analyzing the signals' interactions with both healthy and fractured bones. This technique could potentially be used to track the healing process of the fracture [8-10]. Among the many benefits of microwave imaging are its affordability, portability, and safety. The goal of this study is to demonstrate how it may be applied to develop a simple and efficient method for identifying and tracking bone fractures [6-8]. Using electromagnetic radiation in the microwave frequency range (300 MHz to 300 GHz), microwave imaging (MWI) is a non-invasive method for producing images of objects or tissues. It has been extensively researched for use in medicine, including recognizing brain hemorrhages, evaluating meniscus injuries, and detecting breast cancer in its early stages [9-11].

Unlike X-rays, microwave imaging does not damage tissues because it uses non-ionizing radiation, which is one of its primary benefits. Furthermore, variations in the dielectric characteristics of tissues, such as their conductivity and water content, can be detected by microwaves. This enables the detection of tissue anomalies. Furthermore,

[2] *Corresponding author: [2] Shivesh Tripathi [2]Department of Electronics and Communication Engineering, G L Bajaj Institute of Technology and Management, Gr. Noida

[1] Tilak Dhari Singh and [4]V S Tripathi [1,4] Department of Electronics and Communication Engineering,[5]Motilal Nehru National Institute of Technology, Allahabad, Prayagraj

[3]Kamal Prakash Pandey, [3]Department of Electronics and Communication Engineering, BBS College of Engineering & Technology, Allahabad, Prayagraj

interior tissues and organs can be imaged using microwaves because they can penetrate deeper than ultrasound [12-14]

There has been done several studies based on microwave sensors for detecting bone fracture healing. Some of the studies are explained here. In reference [15], a non-invasive microwave testing has been proposed for the studies of biological tissues. It is widely used due to the benefits of low cost and lower risk of uses. The proposed antenna is operating the range of frequency 8-12 GHz within standard SAR limits [16-17]. In reference [18-19], microwave-based sensor is proposed because of lower level of harm in comparison to others available non-invasive devices, some microwave devices used in near-field for tumour detection have been externally implemented [20]. In few cases, antenna-based Sensors has been integrated with fracture fixation plates as reported in reference [21]. In the early stage of microwave-based bone fracture detection has been used using bulky waveguide components, open-ended rectangular waveguide, and horn antennas. In recent years, the microstrip patch antenna and transmission line based printed antenna have been widely used for detecting dielectric constants of the materials [22]. Ring resonators based printed structures have also been used for permittivity measurement devices for fluids [23]. Defects in dielectric properties have been non-destructively measured by microwave planar antennas. In reference [24], microwave-based sensor has been developed to detect bone fracture by using Electromagnetic Band Gap (EBG) structure in planar antenna and developed a contact with skin of the human body, even that non-uniform nature of skin contact between successive measurement may affect the accuracy of measurement. In reference [25], the regeneration of bone is tested using fabricated symmetrical phantom structure having tibia, fibula, muscle, and fat. In reference [26], a loop based dual band monopole antenna is used for detecting heart failures. Even though, the loop of the resonator is used for optimizing the size of the antenna making it suitable for wearable devices. In reference [27], a monopole antenna with defected ground structure (DGS) has been proposed. A miniaturized textile-based monopole antenna has been proposed in reference [28-29] to detect malignant tumours without skin contact. The proposed antenna is operating the range of frequency 8-12 GHz within standard SAR limits.

II. A ANTENNA DESIGN & SPECIFICATION

Methodology

A. Antenna Setup and Data Acquisition

This technique makes use of a linearly polarized antenna that functions in the bone's near-field area. The antenna collects data at various frequencies between 3.08 and 11.57 GHz by methodically scanning regularly spaced locations. A thorough grasp of how the signals reflect from both healthy and damaged bone structures is made possible by this data collecting process, which guarantees that the microwave signals interact with the bone tissues under a variety of situations [10].

B. Antenna Scanning and Data Acquisition

The antenna is placed a few millimetres above the surface of the bone and moved linearly along it to identify fractures. At i=1, Na, it gathers reflection coefficients, S11(xi,fl), which correlate to particular antenna sites, Pa(xi,y,z). The antenna scans a range of frequencies between 3.08 and 11.57 GHz, l=1, Nf, at each point. Reliable imaging requires precise knowledge of the antenna placements' coordinates, even when regular spacing between them is not necessary [18].

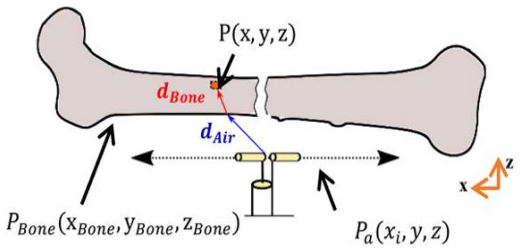

Fig. 1. Representation of the microwave imaging setup with an antenna-operated in radar mode, linear scan on the x-axis, and depth on the z-axis [18]

A broadband Vivaldi antenna is designed for monitoring bone fracture healing.

In this study a broad frequency coverage is made possible by the tapered slot construction of the Vivaldi antenna employed in simulation.

The main components of the antenna design are listed below:

C. Theoretical Model for Microwave Propagation in Bone Fracture Detection

Understanding how microwave signals go through different tissues, especially bones, is the main goal of the theoretical model for microwave propagation in bone fracture diagnosis. This model investigates various tissues' dielectric characteristics, including their capacity to conduct and store electrical energy. Bone, muscle, skin, and other surrounding tissues have different characteristics, which affects how the microwaves interact with them.

D. Microwave Propagation in Tissues

Because every tissue type has various characteristics, microwaves go through them in different ways:

1. **Tissue Properties:** Every tissue, including muscle and bone, has a unique capacity for both conducting and storing electrical energy. For example, compared to softer tissues like muscle or skin, bone usually has a reduced capacity to store electrical energy. When microwaves travel through or meet various tissues, these changes affect how they reflect, transmit, and are absorbed.
2. **Effect of Fractures:** A bone's structure is upset after a fracture, resulting in voids or abnormalities. These modifications have an impact on the behavior of microwaves, changing the patterns of absorption, scattering, and reflection. Since the reflected signals may be used to identify the changed tissue characteristics, the model aids in forecasting how these fractures will affect the microwave signal.
3. **Microwave Interaction with Bone:** Microwaves interact with bone by either being absorbed as they travel through the tissue or reflecting to the antenna. The signal strength varies with tissue depth and fracture severity, and the model considers how microwaves scatter when they strike bone abnormalities like fractures. Because these variances reveal information about the site and severity of the fracture, this is essential for fracture detection.
4. **Wave Propagation Models:** Techniques like ray tracing and finite-difference time-domain (FDTD) are used to model how microwaves move through tissues. These techniques take into consideration variables such how fractures affect the microwave signal, how the signal decreases throughout transmission, and the angle at which microwaves interact with the tissue.
5. **Reflection and Absorption:** A portion of the microwave wave is reflected to the antenna and the remainder is absorbed by the tissue when it meets different types of tissue, such as skin to muscle or muscle to bone. The level of reflection can be used to detect fractures and gives valuable information about the tissue structure. By simulating how fractures alter the reflection pattern, the model provides information about how these modifications affect microwave signals. In conclusion, this theoretical model aids in simulating the interactions of microwaves with bone structures that are both healthy and damaged. It makes it possible to identify and locate bone fractures by comprehending how fractures alter microwave reflection patterns.

Antenna Design

1) Overall Dimensions: The antenna is 28 mm in length, 29.1 mm in breadth, and 1.5 mm in substrate thickness.

2) Substrate Material: Rogers RT/duroid 5880TM, a low-loss dielectric material perfect for high-frequency applications, is used in its construction.

3) Circular Aperture: The antenna's upper section has a 4 mm-diameter circular cut-out.

4) Exponential Taper (Main Curve): A sizable, tapered, curved slot that spans an angle of 47.121° is part of the antenna. This curve's measurements are 12 mm on the y-axis and 14 mm on the x-axis.

5) Straight Section Above the Curve: A straight rectangular segment measuring 9 mm in length and 2 mm in width is located above the tapering curve.

6) Side Cuts: Two rectangular cuts are symmetrically positioned on each side of the antenna design:

7) Top Side Cut: 6 mm × 1 mm

8) Bottom Side Cut: 5 mm × 1 mm

9) Tilted Cuts in the Middle: The tapered slot has two slanted rectangular incisions on either side:

10) Dimensions: 9.434 mm × 1.414 mm each.

11) Tilt Angle: 33.69° from the horizontal plane.

To monitor bone fracture healing, first a phantom model is created for bone as shown in Fig 2 (a).

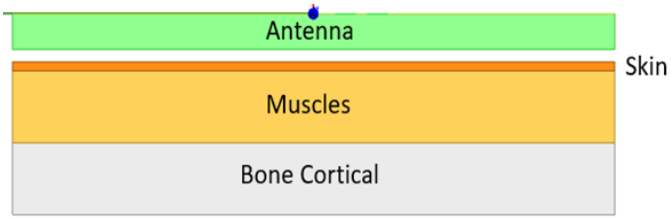

Figure 2(a). Phantom model of bone interacting with antenna

The antenna's feedline has a symmetric L-shaped form, with a 10 mm by 3 mm vertical part and a 10 mm by 3 mm horizontal section. For the best antenna performance, this arrangement maintains constant impedance along the feedline while guaranteeing effective signal transmission.

The bone phantom consists of three layers:

1. Antenna Placement: positioned to send and receive information through the layers of the skin.

2. Skin Layer: 0.4 mm thick, signifying the outermost layer of tissue.

3. Muscle Layer: 3 mm thick, mimicking the bone's surrounding soft tissue.

4. Bone Cortical Layer: Modelling the dense bone tissue, it is 3 mm thick.

By simulating the tissue structure surrounding a bone fracture, this design makes it possible to accurately evaluate microwave imaging for fracture healing shown as Fig. 2 (b).

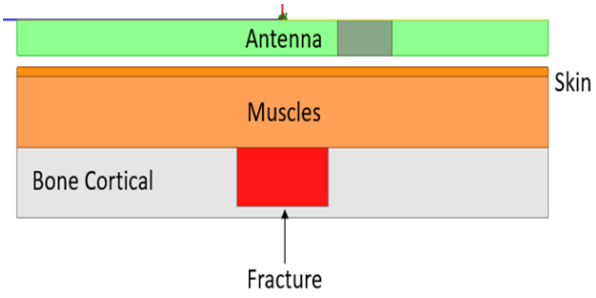

Figure 2(b). Antenna interaction with fractured bone

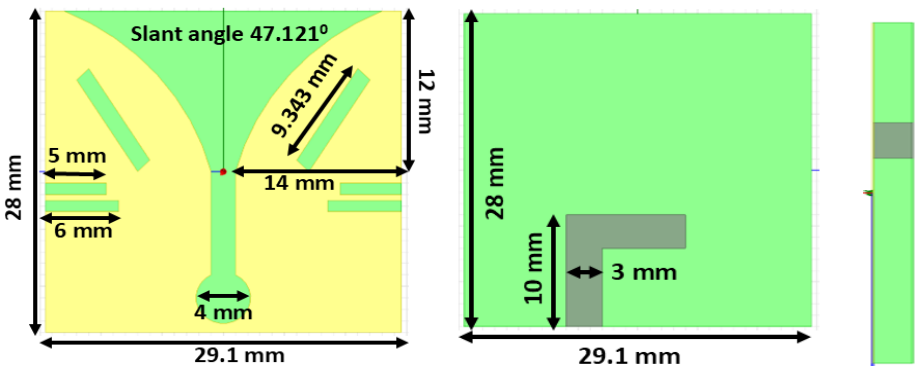

Fig. 3 (a) Patch (b) Ground (c) Port Excitation

To monitor bone fracture, 28 mm x 5 mm x 2.5 mm fracture is modelled near the centre of the bone phantom. Effective testing and imaging of fracture healing are made possible by this dimension, which precisely depicts the size and shape of a normal bone fracture.

III. RESULT AND DISCUSSION

A. Simulated Results

Proposed antenna is simulated using ansys HFSS version 23. An examination of the S11 characteristics shows Fig 4 (a) that the antenna is responsive in the frequency ranges of 3.08–11.57 GHz and 14.90–20.87 GHz, which can both be utilized as potential bandwidths for our experiment. After careful consideration, we have chosen to carry out our experiment using a resonance frequency of 4.8 GHz in the 3.08–11.57 GHz range.

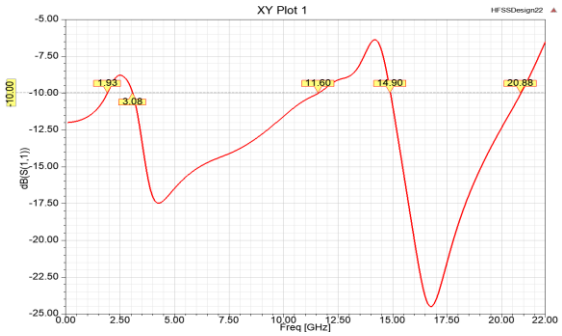

Fig. 4 (a). S11 graph with respect to frequency

In fig. 4 (b), the Gain vs. Frequency figure illustrates how the antenna's gain, or ability to focus radiation in a particular direction, changes with frequency. The gain is expressed in decibels (dBi) and plotted against the frequency in gigahertz (GHz). We can observe that the gain remains rather constant over the selected frequency range of 3.08–11.57 GHz. Because of its stability in gain, which ensures consistent performance over the whole spectrum, the antenna can be utilized for accurate measurements during the fracture healing processed chosen to carry out our experiment using a resonance frequency of 4.8 GHz in the 3.08–11.57 GHz range.

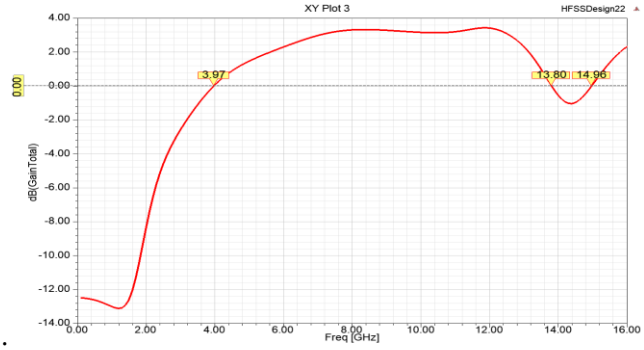

Fig. 4 (b). Gain verses frequency graph

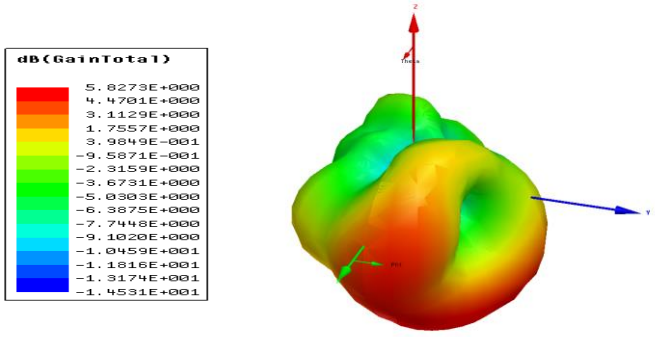

Fig. 5 (a). 3D polar plot of gain

The 3D Gain Plot provides a three-dimensional depiction of the energy radiation from the antenna in different directions.

It enables us to assess the radiation pattern's main lobe width and the antenna's ability to concentrate energy in the intended direction shows 5 (a). Fig. 5 (b) shows E-field radiation pattern of antenna. The antenna's energy radiation at various angles is displayed in the Radiation Pattern Plot.

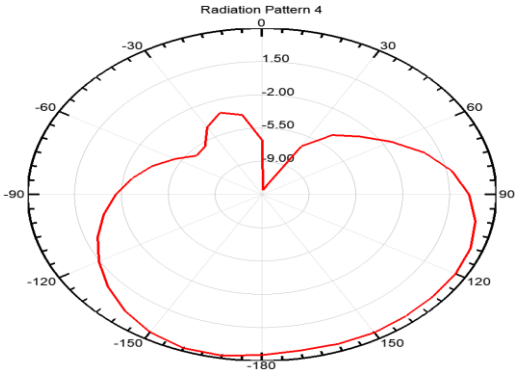

Figure 5 (b). E- field radiation pattern

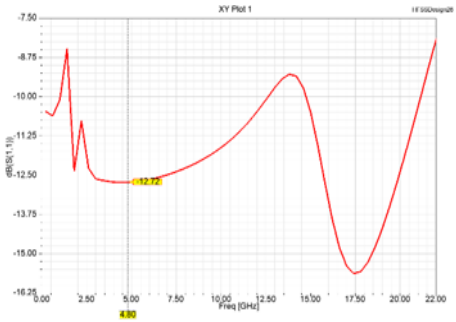

Fig. 6 (a). Fracture healing phase 1 (0 % healed)

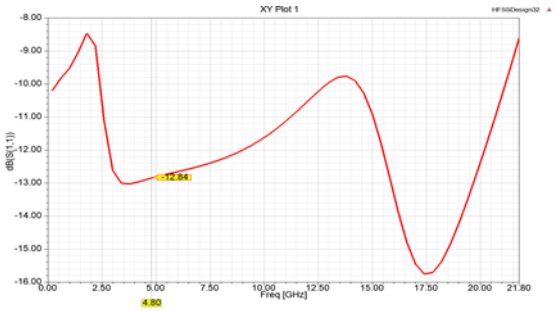

Fig. 6 (b). Fracture healing phase 2 (20 % healed)

1. Fracture healing phase 1 (0 % healed)

The fluidity of the blood, which is necessary to provide the conditions necessary for tissue regeneration and the early phases of healing, is reflected in these values as shown in fig. 6 (a).

2. Fracture healing phase 2 (20 % healed)

The healing process advances in the second phase as a mixture of blood and bone cells starts to fill the fracture site. As a result of this combination, the conductivity drops to 4.2874, and the permittivity drops to 45.4662. The nature of the tissue changes when bone cells begin to proliferate, which is a critical phase in the creation of new bone tissue and more fracture stabilization as shown in Fig. 6(b).

3. Fracture healing phase 3 (40 % healed)

As more bone cells are added to the mixture of blood and cellular material, the fracture site continues to repair during the third phase. As this process progresses, the conductivity falls to 3.4442 and the permittivity further declines to 36.6334. Even though the bone matrix is not yet completely healed, this stage shows that the healing process is moving forward and that it is becoming more cohesive and structured are shown in Fig. 6 (c).

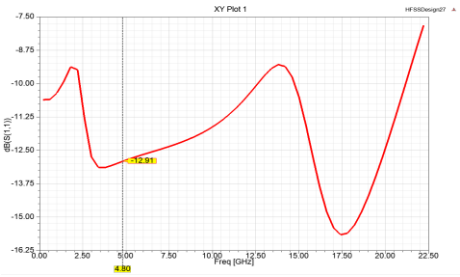

Fig.6 (c) Fracture healing phase 3 (40 % healed)

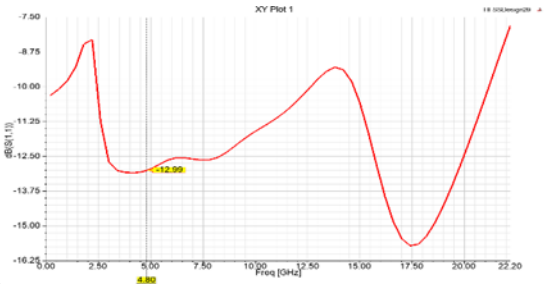

Fig. 6 (d). Fracture healing phase 4 (60 % healed)

4.Fracture healing phase 4 (60 % healed)

The fourth phase is characterized by a more solid mixture of bone cells and blood as the fracture site continues to heal with increased bone cell activity. The conductivity falls to 2.6010 and the permittivity further reduces to 27.8006. This stage shows in figure 6(d) how the bone tissue is continuing to mature; although some tissue remodelling is still necessary, the area starts to resemble fully healed bone.

5. Fracture healing phase 5 (80 % healed)

The fracture site has little blood and is primarily composed of bone cells at the fifth and final stage of healing. At this stage, the fracture site is almost fully healed and the bone is getting closer to stable shape, as shown by the permittivity of 18.9678 and the conductivity of 1.7579. At this stage, the bone tissue is completely restored and structurally sound, signifying the end of the healing process as shown in Fig. 6 (e).

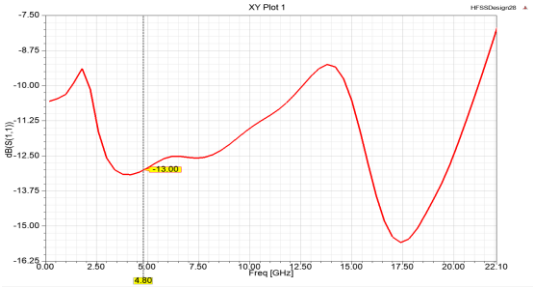

Fig. 6 (e). Fracture healing phase 5 (80 % healed)

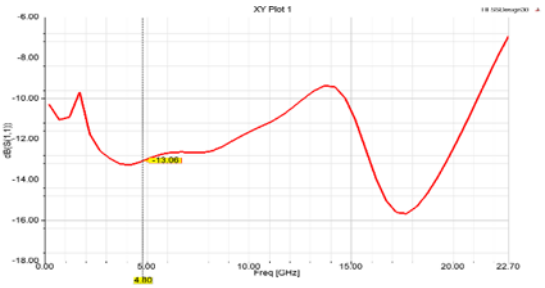

Fig. 6 (f). Fracture healing phase 6 (100 % healed)

6. Fracture healing phase 6 (100 % healed)

The bone has fully recovered from the fracture location and returned to its stable, natural shape during the sixth and last stage of healing shows in Fig. 6 (f). The bone tissue is now fully functioning and restored, with characteristics like those of normal bone. A permittivity of 10.1350 and a conductivity of 0.9147 show that the healing process is complete and the bone has returned to its normal form.

B. Antenna Measurement Result

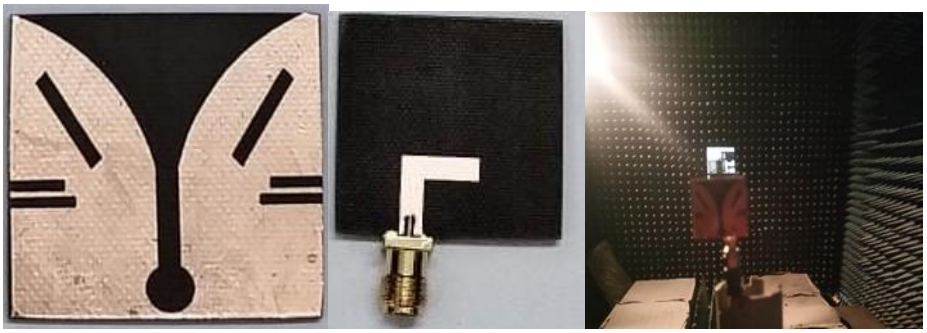

(a) (b) (c)

Figure 7. Fabricated antenna (a) Top side (b) bottom side (c) Measurement in anechoic chamber.

In Fig. 7, the fabricated antenna has been shown. After fabrication the antenna is measured using VNA in anechoic chamber. The fabricated antenna also has been tested with mimicking gel to validate the phantom model of skin, fat, muscle, and bone respectively as shown in Fig.8.

Fig. 8. Experimental setup for mimicking gel for skin, fat, muscle, and bone phantom.

In Fig.8, the semi liquid mimicking gel is prepared by using Tx-100, distilled water and NACl in different proportion. The proposed gel representing different tissue layers are further experimentally tested with proposed antenna to indicate the variation in reflection coefficient to show the different healing level. To indicate the different healing level, the mixture of NaCl is used in different amount from 10-40 grams.

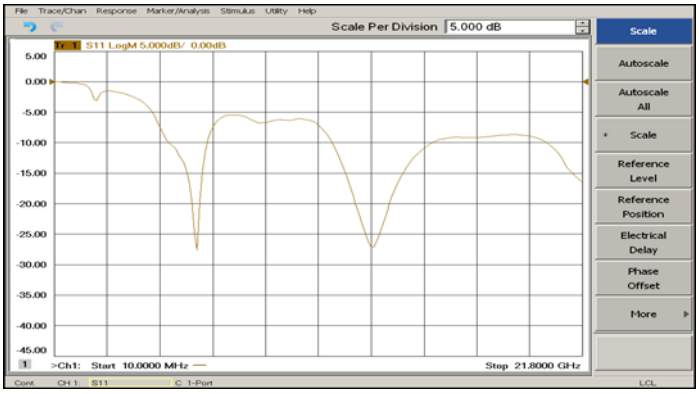

Fig. 9 shows measured result of reflection coefficient S_{11}

In Fig. 9, measured result of reflection coefficient S_{11} has been shown.

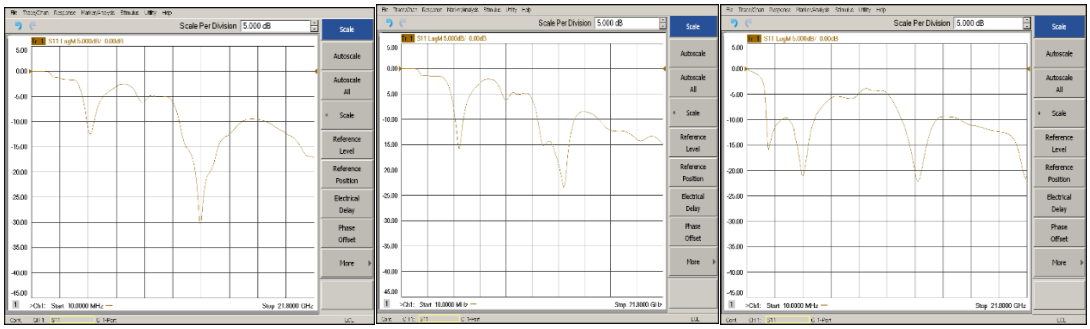

(a) (b) (c)

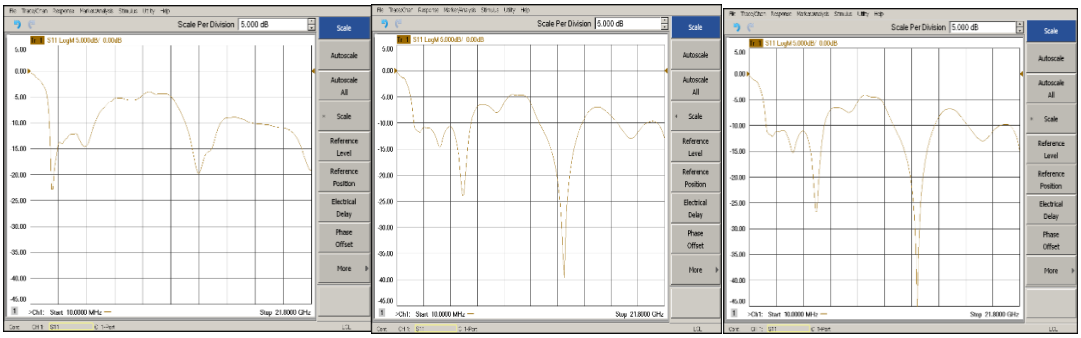

(d) (e) (f)

Fig. 10 shows the measured result is approximately aligned.

Figure 10 shows the experimental results for monitoring of bone fracture healing from stage 1 to stage 6 as already discussed in fracture healing phase. Fig.10 (a) show the variation in reflection coefficient of -12 dB for phase 1 healing level. Fig. 10 (b) show -15dB S_{11} for phase 2 healing. Figure 10 (c) has –20 dB S_{11} for phase 3, Fig. 10 (d) show -22 dB S_{11} for phase 4. In Fig.10 (e) e -24 dB S_{11} is found for phase 5 and finally -26dB S_{11} is observed for phase 6 in Fig. 10 (f). Which shows 100% level of reconstructed bone.

TABLE 1. S_{11} values at 4.8 GHz during different phases of bone fracture healing

Phases	**Relative Permittivity (ε_r)**	**Loss tangent (tanδ)**	**Conductivity σ in S/m**	**S_{11} Value in dB (at 4.8GHz)**
Phase 1 (0% Healed)	54.299	0.35384	5.1306	-12
Phase 2 (20% Healed)	45.4662	0.350668	4.287416	-15
Phase 3 (40% Healed)	36.6334	0.347496	3.444232	-20
Phase 4 (60% Healed)	27.8006	0.344324	2.601048	-22
Phase 5 (80% Healed)	18.9678	0.341152	1.757864	–24
Phase 6 100% Healed)	10.135	0.33798	0.91468	-26

TABLE 2. Comparison of proposed work with other existing work

Reference	**Substrate/ Dimension (mm^3)**	**Resonant Frequency/ Bandwidth [GHz]**	**Measured Technique**	**Measured value**
[3]	Rogers RT duroid/ 25×25×0.25	4.8/ 1.2	S_{11}	Shift in frequency/ sensitivity of 4 MHz/εr
[19]	FR-4/ 18×19×0.8	3.76, 6.7, 9.8/ 3.14-11.7	S_{11}, SAR	1.6 w/kg for 1g at 18 dBm I/P power
[20]	FR-4 Glass Epoxy/ 114×80	2.45/ 0.292	S_{11}/ S_{21}	Accuracy 98.86 by using

				Lanczos method
[21]	Rogers RT/duriod 5880/ 30×40×1.016	3.4/0.5	S_{11}	Propagation delay (ns)
[22]	FR-4/ 32× 30×1.6	2.45/ 0.027	S_{11}	Shift in frequency
Proposed work	Rogers RT/duroid 5880TM/ 28×29.1×1.5	3.08–11.57 GHz and 14.90–20.87 GHz	S_{11}	Shift in frequency/ amplitude shift in S_{11}

CONCLUSION

In this study, a Vivaldi antenna-based microwave sensor has been developed for monitoring bone fracture healing. The proposed antenna is simulated using ansys HFSS electromagnetic suite software and experimentally tested in anechoic chamber. The proposed antenna has the overall dimension of 28×29.1×1.5 mm^3 which is very compact in size and fabricated on the substrate Rogers RT/duroid 5880TM. The antenna resonates at 4.8 and 17 GHz frequency in frequency ranges of 3.08–11.57 GHz and 14.90–20.87 GHz respectively. Almost 3 dBi gain is found stable inside the desired band in free space. Hence proposed antenna is suitable monitoring bone fracture healing from phase 1 to phase 6 of fractured bone in terms of percentage of healing from 0% to 100%.

REFERENCES

1. Santos, K. C., Fernandes, C. A., & Costa, J. R. (2022, March). Experimental evaluation of thin bone fracture detection using microwave imaging. In 2022 *16th European Conference on Antennas and Propagation (EuCAP)*, pp. 1-3. IEEE.
2. Santos, K. C., Fernandes, C. A., & Costa, J. R. (2023). Validation of a compact microwave imaging system for bone fracture detection. *IEEE Access*, 11, 63690-63700.
3. Singh, T., Mishra, P. K., Verma, A., Siddhi, S., Sharma, P., & Tripathi, V. S. (2024, February). A Trapezoidal Ground-based Truncated Rectangular Patch Antenna for Non-Invasive Monitoring of Bone Fracture Healing. In *2024 IEEE Wireless Antenna and Microwave Symposium (WAMS)* pp. 1-5.
4. Jacob, N. E., & Wyawahare, M. V. (2013). Survey of bone fracture detection techniques. *International Journal of Computer Applications*, *71*(17).
5. Chandra, R., Zhou, H., Balasingham, I., & Narayanan, R. M. (2015). On the opportunities and challenges in microwave medical sensing and imaging. *IEEE transactions on biomedical engineering*, *62*(7), 1667-1682.
6. Lodato, R., & Marrocco, G. (2015). Close integration of a UHF-RFID transponder into a limb prosthesis for tracking and sensing. *IEEE Sensors Journal*, *16*(6), 1806-1813.
7. Mirza, A. F., See, C. H., Danjuma, I. M., Asif, R., Abd-Alhameed, R. A., Noras, J. M., ... & Excell, P. S. (2017). An active microwave sensor for near field imaging. *IEEE Sensors Journal*, *17*(9), 2749-2757.
8. Oess, N. P., Weisse, B., & Nelson, B. J. (2009). Magnetoelastic strain sensor for optimized assessment of bone fracture fixation. *IEEE Sensors Journal*, *9*(8), 961-968.
9. Oess, N. P., Weisse, B., & Nelson, B. J. (2009). Magnetoelastic strain sensor for optimized assessment of bone fracture fixation. *IEEE Sensors Journal*, *9*(8), 961-968.
10. Li, Y., Bowler, N., & Johnson, D. B. (2010). A resonant microwave patch sensor for detection of layer thickness or permittivity variations in multilayered dielectric structures. *IEEE Sensors Journal*, *11*(1), 5-15.
11. Subbaraj, S., Ramalingam, V. S., Kanagasabai, M., Sundarsingh, E. F., Selvam, Y. P., & Kingsley, S. (2016). Electromagnetic nondestructive material characterization of dielectrics using EBG based planar transmission line sensor. *IEEE Sensors Journal*, *16*(19), 7081-7087.
12. Stegeman, T., Pfeiffenberger, A. H., Bailey, J. P., & Hamilton, M. C. (2014). Broadband characterisation of engineered dielectric fluids using microstrip ring resonator technique. *Electronics letters*, *50*(8), 576-578.
13. Ramalingam, V. S., Kanagasabai, M., & Sundarsingh, E. F. (2019). A compact microwave device for fracture diagnosis of the human tibia. *IEEE Transactions on Components, Packaging and Manufacturing Technology*, *9*(4), 661-668.
14. G. Ruvio, A. Cuccaro, R. Solimene, A. Brancaccio, B. Basile, and M. J. Ammann, ‘‘Microwave bone imaging: A preliminary scanning system for proof-of-concept,’’ Healthcare Technol. Lett., vol. 3, no. 3, pp. 218–221, Sep. 2016.

15. Rezaeieh, S. A., Abbosh, A., & Wang, Y. (2014). Wideband unidirectional antenna of folded structure in microwave system for early detection of congestive heart failure. *IEEE transactions on antennas and propagation*, *62*(10), 5375-5381.
16. Ojaroudi, N., Ojaroudi, M., & Ghadimi, N. (2012). UWB omnidirectional square monopole antenna for use in circular cylindrical microwave imaging systems. *IEEE Antennas and Wireless Propagation Letters*, *11*, 1350-1353.
17. Mersani, A., Osman, L., & Ribero, J. M. (2019). Flexible UWB AMC antenna for early-stage skin cancer identification. *Progress In Electromagnetics Research M*, *80*, 71-81.
18. Santos, K. C., Fernandes, C. A., & Costa, J. R. (2022). Feasibility of bone fracture detection using microwave imaging. *IEEE Open Journal of Antennas and Propagation*, *3*, 836-847.
19. Rizwan, S., Phani Kumar, K. V., & Palaniswamy, S. K. (2023). On the Experimental Investigation of Bone Fracture Recovery Process Using an Ultra-Wideband Planar Monopole Antenna. *International Journal of Antennas and Propagation*, *2023*(1), 8825446.
20. Ramalingam, V. S., Kanagasabai, M., & Sundarsingh, E. F. (2019). A compact microwave device for fracture diagnosis of the human tibia. *IEEE Transactions on Components, Packaging and Manufacturing Technology*, *9*(4), 661-668.
21. Kerketta, S. R., & Ghosh, D. (2020). Microwave sensing for human bone health evaluation. *AEU-International Journal of Electronics and Communications*, *127*, 153469.
22. Boologam, A. V., Krishnan, K., Palaniswamy, S. K., Kumar, S., Bhowmik, S., Sharma, N., ... & Chatterjee, S. (2022). On the design and development of planar monopole antenna for bone crack/void detection. *International Journal of Antennas and Propagation*, *2022*(1), 4663488.
23. Tripathi, S., Pathak, N. P., & Parida, M. (2019). A dual feed PIN diode based switchable multiband planar meandered antenna for intelligent transportation system application. *International Journal of RF and Microwave Computer-Aided Engineering*, *29*(11), e21936.
24. Raj, S., Mishra, P. K., Tripathi, S., & Tripathi, V. (2022). A Defected Ground Structure Based Compact Circular Patch Antenna Design for mm Wave Application. *Defence Science Journal*, *72*(4), 592-599.
25. Tripathi, S., Pathak, N. P., & Parida, M. (2016). Microwave front-end subsystems design for ITS/GPS applications. *Engineering Science and Technology, an International Journal*, *19*(4), 1815-1825.
26. Raj, S., Tripathi, S., Upadhyay, G., Tripathi, S. S., & Tripathi, V. S. (2021). An electromagnetic band gap-based complementary split ring resonator loaded patch antenna for glucose level measurement. *IEEE Sensors Journal*, *21*(20), 22679-22687.
27. Tripathi, S., Pathak, N. P., & Parida, M. (2019). Concurrent Dual-Band Double-Layer High Gain Planar Antenna for WAICs/ITS Application. In *Computing, Communication and Signal Processing: Proceedings of ICCASP 2018* (pp. 37-46). Springer Singapore.
28. Tripathi, S., Pathak, N. P., & Parida, M. (2018, November). Dual-band dual-beam microstrip patch antenna for intelligent transportation systems application. In *2018 5th IEEE Uttar Pradesh Section International Conference on Electrical, Electronics and Computer Engineering (UPCON)* (pp. 1-5). IEEE.
29. Tripathi, S., Pathak, N. P., & Parida, M. (2019). Symmetrical double-comb multi-slotted large bandwidth antenna for intelligent transportation systems. *International Journal of RF and Microwave Computer-Aided Engineering*, *29*(1), e21471.